Journal of Dynamics, Monitoring and Diagnostics, 2022, 1, 57-65
https://doi.org/10.37965/jdmd.2022.57

ISTP
RESEARCH ARTICLE

Rolling Bearing Condition Monitoring Technique Based on Cage Rotation Analysis and Acoustic Emission

Matías Marticorena[1,2] and Oscar García Peyrano[2]
[1]Vibrations Laboratory, Vibrations Division, National Atomic Energy Commission, San Carlos de Bariloche, Argentina
[2]Balseiro Institute, Cuyo National University, San Carlos de Bariloche, Argentina

(Received 12 November 2021; Revised 07 February 2022; Accepted 22 February 2022; Published online 07 March 2022)

Abstract: In this paper, we present an alternative technique for detecting changes in the operating conditions of rolling element bearings (REBs) that can lead to premature failure. The developed technique is based on measuring the kinematics of the bearing cage. The rotational motion of the cage is driven by traction forces generated in the contacts of the rolling elements with the races. It is known that the cage angular frequency relative to shaft angular frequency depends on the bearing load, the bearing speed, and the lubrication condition since these factors determine the lubricant film thickness and the associated traction forces. Since a large percentage of REB failures are due to misalignment or lubrication problems, any evidence of these conditions should be interpreted as an incipient fault. In this paper, a novel method for the measurement of the instantaneous angular speed (IAS) of the cage is developed. The method is evaluated in a deep groove ball bearing test rig equipped with a cage IAS sensor, as well as a custom acoustic emission (AE) transducer and a piezoelectric accelerometer. The IAS of the cage is analyzed under different bearing loads and shaft speeds, showing the dependence of the cage angular speed with the calculated lubricant film thickness. Typical bearing faulty operating conditions (mixed lubrication regime, lubricant depletion, and misalignment) are recreated. It is shown that the cage IAS is dependent on the lubrication regime and is sensitive to misalignment. The AE signal is also used to evaluate the lubrication regime. Experimental results suggest that the proposed technique can be used as a condition monitoring tool in industrial environments to detect abnormal REB conditions that may lead to premature failure.

Keywords: Acoustic emission; cage instantaneous angular speed; condition monitoring; cyclostationary analysis; rolling element bearing

I. INTRODUCTION

Rolling element bearings (REBs) are one of the most common elements found in rotating machinery, and their failure continues to be a frequent cause for machine downtime. Since the 1970s, several bearing fault detection techniques have been developed [1,2]. Nowadays, vibration-based condition monitoring (CM) is a mature technique for fault detection and assessment in REB [3,4]. Advanced diagnostic techniques are constantly being developed for early failure detection, with the aim of detecting vibration signals generated by incipient faults. Current vibration-based techniques are not well suited to detect operating conditions that can lead to premature failure before damage initiation, such as lubrication problems or REB misalignment, as these techniques are based on vibration signals originated at the race-rolling elements discontinuities. Industry statistics show that 50% of REB failures are due to lubrication problems and contamination [5], that is, the inability of the lubricant to form a sufficient film on the contact surfaces between rolling elements and races. Therefore, it is of great interest to develop CM techniques capable of detecting lubrication problems before surface damage occurs. There are recent studies on the use of the acoustic emission (AE) technique to detect changes in the tribological parameters of machine elements for CM and wear detection [6–8], but this is not yet a mature technique.

A recent development for CM is the cyclostationary analysis [9]. As stated by Antoni et al., a cyclostationary signal is one that exhibits some hidden periodicity of its energy flow and the vibration signals from rotating machines pertain to this group. This makes cyclostationarity a powerful framework in vibration-based CM, because of its ability to describe the statistical behavior of faults in the form of symptomatic modulations or repetition of transients [10].

The analysis of the instantaneous angular speed (IAS) has been studied for fault detection in pumps [11], turbines [12], diesel engines [13], induction motors [14], and REBs [15,16], among others. Usually, the IAS is obtained from an encoder signal, although some authors have obtained IAS from vibration signals [16] or using some feature of the rotating machine as an encoder [11]. In all presented cases, the analysis is carried out using the shaft IAS. The different techniques for the computation of IAS and associated errors have been presented by Li et al [17], while the precision in the spectral domain has been studied by André et al [18].

The problem of the dynamic behavior of REBs under elastohydrodynamic lubrication has been theoretically and experimentally addressed since the 1960s [19,20] and is well understood that cage dynamics plays a major role in REB behavior. The interest in cage dynamics has been mainly motivated by the instability problem found in certain speeds, loads, and lubrication conditions [20–24]. It is known that the cage angular frequency relative to shaft

Corresponding author: Matías Marticorena (matias.marticorena@cab.cnea.gov.ar).

angular frequency is dependent on the contact angle, the bearing load, the bearing speed, and the lubrication condition, since these are determinant factors for the lubricant film thickness and the associated traction forces [20,25]. Some authors have developed precise methods for measuring the cage trajectory [22,26] and cage rotating speed [24], but these are techniques for laboratory measurements, not suited for CM applications.

This paper proposes a CM technique for REB based on the cage IAS analysis and AE analysis, as an alternative for classical vibration-based techniques. A first experimental approach is presented, aiming to detect critical operating conditions that can lead to premature failure before damage is initiated.

The rotational motion of the cage is driven by the orbital motion of the rolling elements, which in turn are driven by the traction forces produced by the contact of the rolling elements with the races. Therefore, at constant shaft speed and load, a measured change in the cage IAS can be a symptom of a lubrication problem or a geometrical perturbation (misalignment).

A method for the online measurement of the cage IAS is presented and tested in a test rig using a 6209 ball bearing under different operating conditions and with imposed lubrication problems.

II. METHODOLOGY

A. EXPERIMENTAL SETUP

The experimental validation of the method is conducted using a REB test rig (Fig. 1). It is designed for testing bearings with sizes up to 160 mm outer diameter. The driving force is provided with a three-phase squirrel cage electric motor with a variable frequency drive for control of the angular speed of the shaft. The REB is mounted on a test housing (red part in the left of Fig. 1), and the axial and radial loading is accomplished through weights and a lever mechanism. A 256-point incremental encoder is mounted on the shaft, and a Brüel & Kjaer 4371 accelerometer is radially attached to the test housing.

Fig. 2 shows the test bearing mounted on the shaft (left photo) and the metal adaptor used as an interface to the test housing (right photo). Two specially designed sensors are mounted on the adaptor: a piezoelectric transducer for measuring high-frequency stress waves, denoted as *acoustic emission* in this context, and a cage sensor to measure the distance from the fixed adaptor to the metal cage.

Fig. 1. Rolling element bearing test rig.

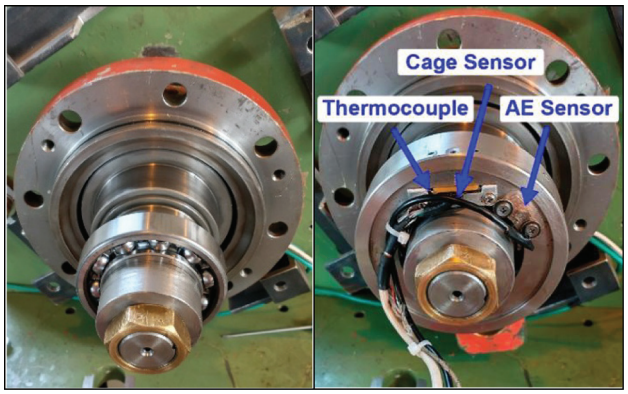

Fig. 2. Left: Test ball bearing installed on the shaft. Right: Ball bearing support with sensors installed.

The cage sensor shown in Fig. 3 is a device designed ad-hoc. It consists of a magnetic field magnetoresistive transducer and a permanent magnet mounted adjacent to the transducer. Fig. 4 presents a schematic diagram with the calculated magnetic flux lines for two different angular positions of the cage. The field of the permanent magnet is disturbed by the rotation of the cage when a cage pocket passes in front of the magnet. The signal generated by the transducer, shown in Fig. 6, is used to calculate the cage rotation and will be explained later.

The high-frequency piezoelectric is located adjacent to the load zone of the bearing. This is important because of the short attenuation length associated with high-frequency stress waves. It is connected to a preamplifier with 60 dB gain and to an analog 50 kHz – 250 kHz passband filter. The accelerometer signal is filtered with a 15 kHz lowpass filter.

The tests were conducted using a 6209 ball bearing with $N = 10$ balls and stamped sheet steel cages. The lubricant is an automotive transmission fluid (Castrol ATF Multivehicle) with the following properties: kinematic viscosity (40 °C) $35 mm^2/s$, density 0.85 g/cm^3, and typical pressure–viscosity coefficient 0.02 mm^2/N.

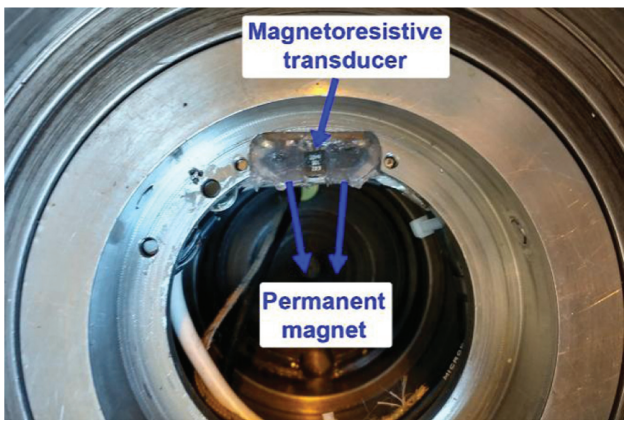

Fig. 3. Detail of the cage sensor. The assembly is protected by silicon rubber.

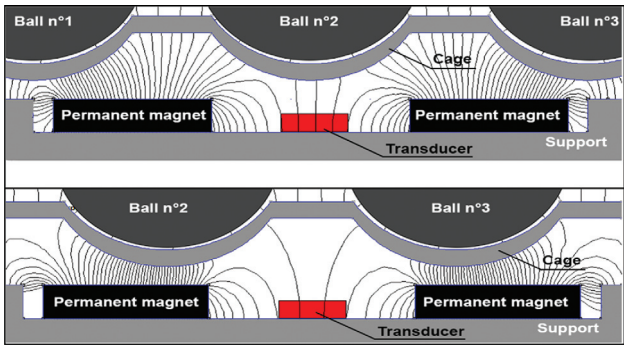

Fig. 4. Diagram showing the magnetic flux lines for two different angular positions of the cage.

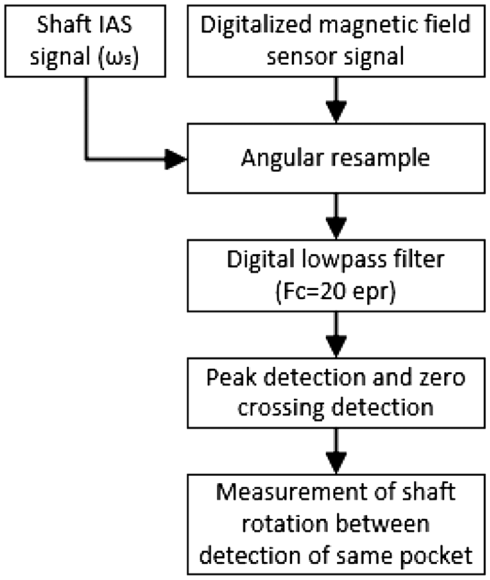

Fig. 5. Flowchart for the calculation of ω_c.

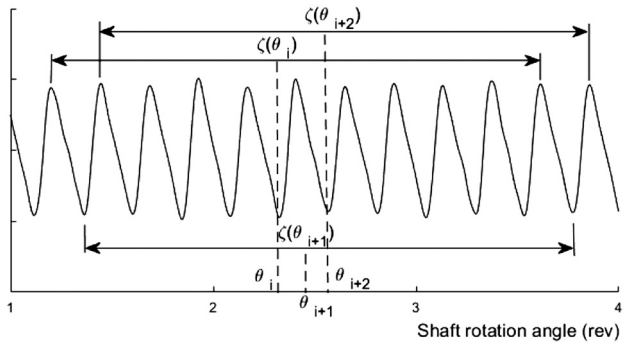

Fig. 6. Measurements on the angular resampled cage sensor signal.

B. MEASUREMENTS AND DATA PROCESSING

The signals were digitalized with a high-frequency ADC ($Fs = 700\ kHz$) and resampled in the angular domain using the shaft encoder. The angle is expressed in shaft revolutions (*rev*). We adopt the definitions of Rémond et al. [27], who proposed to use the term *angle frequency* to define the abscissa axis in the Fourier transform of angular sampled signals and to use the unit *event per rev* (*epr*) defined by the number of events over one angular revolution.

The IAS of the shaft (ω_s) is determined from the digitalized encoder signal using the elapsed time (ET) method presented by Li et al [17], that is, by measuring the ET between successive pulses of the encoder.

The IAS of the cage (ω_c) is determined from the angular resampled digital signal of the cage sensor, by measuring the shaft rotation (in revolutions) between two instances of the detection of a given cage pocket (360° apart). Local maxima, minima, and zero crossing of the cage sensor signal are used. Fig. 5 shows a flowchart of the calculation process. A digital lowpass filter is used to minimize the effect of measurement noise.

The signal from consecutive cage pockets is not employed in this calculation as geometric differences between the pockets would lead to increased uncertainty.

Fig. 6 presents the cage sensor signal resampled in the angular domain as a function of the shaft rotation angle. Each cycle of the signal corresponds to a cage pocket passing in front of the fixed cage sensor. Noting ζ as the elapsed angle between signal maxima, minima, or zero crossing, the cage angle frequency is calculated as:

$$\omega_c(\theta_i) = \frac{1}{\zeta(\theta_i)} \tag{1}$$

Four points per each cage pocket are considered for the ET measurement, so the equivalent sampling frequency of ω_c in the angular domain is $Fs = 4N \cdot \omega_c$, where N is the number of rotating elements. For 6209 ball bearings, $\omega_c \cong 0.4\omega_s$; therefore, $Fs \cong 16\omega_s = 16$ erev.

According to Li et al [17], there are three sources of error in the IAS calculation by the ET method: a) the counting error for the ET, b) the variation of the encoder nominal equidistance, and c) the instability of the clock frequency. In the presented method, there is no variation in the nominal equidistance because the measurement is made between two successive detections of a given cage pocket, as explained earlier. The instability of the clock frequency is considered negligible. Since the maximum counting error for the ET is 1, the maximum relative error of the IAS can be calculated as [17]:

$$\varepsilon = \frac{\omega M}{f_{cl}} \tag{2}$$

where ω is the rotational speed, M is the number of cycles of the encoder, and f_{cl} is the clock frequency. It is worth noting that according to this formula the relative measurement error linearly increases with rotational speed and encoder resolution. For the cage IAS: $\omega = \omega_c \cong 10Hz$ (shaft rotational speed = 25 Hz), $M = 1$, and $f_{cl} = 700\ kHz$; therefore, the relative maximum error for the cage IAS becomes $\epsilon_c =$ 1.4 E-5. The estimated maximum absolute error is

$$\Delta\omega_c = \varepsilon_c\omega_c = 6\text{E} - 6 \text{ erev} \tag{3}$$

Since the sample bearing has no localized faults, the traditional envelope may not be an appropriate tool for analyzing either the acceleration signals or the AE signals, as the envelope is best suited for detecting periodic impulses. For this analysis, a cyclostationary approach is used, based on the algorithm for the fast computation of the

spectral correlation (SC) proposed by Antoni et al. [10]. The SC is computed for the angular resampled acceleration and AE signals, and a modified version of the SC-based enhanced envelope spectrum (EES) [10] is used to describe the periodicity of energy flow at the characteristic bearing frequencies: ball spin frequency (BSF), ball failure frequency (BFF), ball pass frequency – outer race (BPFO), and ball pass frequency - inner race (BPFI). The EES used in this paper is

$$EES_x(\alpha) = \int_{f_1}^{f_2} |S_x(\alpha,f)|df \tag{4}$$

where x is the time signal, S_x is the *spectral correlation* of x (as defined in [10]), α is the angle frequency, f is the traditional spectral frequency, and f_1, f_2 is the desired frequency band for the envelope computation. The EES has the squared units of the signal.

The EES_x is computed for the accelerometer signal ($f_1 = 2$ kHz, $f_2 = 15$ kHz) and the AE signal ($f_1 = 40$ kHz, $f_2 = 250$ kHz).

III. CONDUCTED TESTS

The objective of the tests is to study the behavior of the cage IAS and AE signals under different speed and lubrication conditions, producing different lubricant film thicknesses and therefore different traction forces.

Three tests were conducted: test A aims to evaluate the cage IAS and AE behavior under different speeds producing a change in lubrication regime, from full film to boundary. Test B consists of a loss of lubricant at constant speed and load, producing a transition between full film and boundary lubrication. In test C, a misalignment is imposed, applying an external torque over the vertical axis of the outer race. The bearing behavior is monitored during the imposed misalignment. In all cases, the accelerometer signal is used for comparison, as it is the most common sensor for CM. Table 1 summarizes the test conditions.

The characteristic frequencies for the test bearing were calculated assuming pure rolling and a contact angle of 0°. The obtained frequencies are BSF = 2.55 epr; BPFO = 4.05 epr; BFF = 5.1 epr; BPFI = 5.95 epr.

For the conditions of test A, the minimum film thickness h_{min} is calculated based on the formula derived by Hamrock and Dowson [28]:

Table 1. Conducted tests

Test id.	Description	Test conditions
A	Varying lambda ratio	Shaft speed: 5, 10, 15, 20, and 25 Hz
		Radial load: 12 kN
		Axial load: 3 kN
		Lubricated
B	Lubricant depletion	Shaft speed: 25 Hz
		Radial load: 12 kN
		Axial load: 3 kN
		Loss of lubricant
C	Misalignment	Shaft speed: 25 Hz
		Radial load: 4.5 kN
		Axial load: 0 kN

Table 2. Calculated minimum film thickness and film parameter for test A.

Shaft speed (Hz)	Inner race		Outer race	
	h_{min} (μm)	Λ	h_{min} (μm)	Λ
5	0.08	0.56	0.10	0.69
10	0.13	0.90	0.16	1.1
15	0.17	1.2	0.20	1.4
20	0.20	1.4	0.25	1.8
25	0.24	1.7	0.29	2.0

$$H_{min} = \frac{h_{min}}{R_x} = 3.63U^{0.68}G^{0.49}W^{-0.073}(1 - e^{-0.68\kappa}) \tag{5}$$

where H_{min} is the dimensionless film thickness, U is the dimensionless speed, G is the dimensionless material parameter, W is the dimensionless load, κ is the contact ellipticity ratio, and R_x is the effective radius. The film parameter (or lambda ratio) $\Lambda = h_{min}/\sigma$ is calculated assuming a typical value for the combined surface roughness $\sigma = 0.14$ μm [29]. Table 2 presents the calculated values of h_{min} and Λ for test A.

It is widely accepted that the lubrication regime can be described by the value of Λ and is a common practice among researchers to assume full-film lubrication for $\Lambda > 3$, mixed lubrication for $1 < \Lambda < 3$, and boundary lubrication for $\Lambda < 1$ [6,7]. However, as presented by Greenwood in an extensive review [30], such limits are perhaps overly conservative. There is evidence that full-film lubrication can exist with Λ as low as 1, and values $1 < \Lambda < 2$ are usual in practical applications. The operating conditions in Table 2 were selected to achieve Λ from 0.5 to 2, with the hypothesis that mixed lubrication with metal to metal contact is to be expected for $\Lambda < 1$.

IV. RESULTS

A. TEST A RESULTS: VARYING LAMBDA RATIO

The cage IAS for the five shafts speeds is presented in Fig. 7. Fig. 8 shows the most relevant calculated features for test A: cage IAS (ω_c), rms and kurtosis for the AE signal; rms and kurtosis for the accelerometer signal.

The mean value of ω_c differs significantly for the condition for which mixed lubrication is expected ($\omega_s = 5\ Hz$). The standard deviation of ω_c is higher for $\omega_s = 5\ Hz$, denoting major variability of cage IAS as can be seen in Fig. 7. This variability can be caused by variable traction forces due to eventual metal to metal contact in the mixed lubrication regime. This is compatible with the observation of Nogi et al. [23], where instability is more likely to occur under high-load and low-speed conditions due to less ball-race sliding. It is worth noting that mean cage IAS is clearly different between $\omega_s = 5\ Hz$ and $\omega_s = 10\ Hz$ (Fig. 8) where the transition from mixed lubrication to boundary lubrication is expected based on calculated lambda ratio.

The high kurtosis of the AE signal for $\omega_s = 5\ Hz$ indicates the presence of impulsive stress waves and could also be a symptom of asperities interaction within the ball-race contact. Fig. 9 presents a comparison of the AE signal

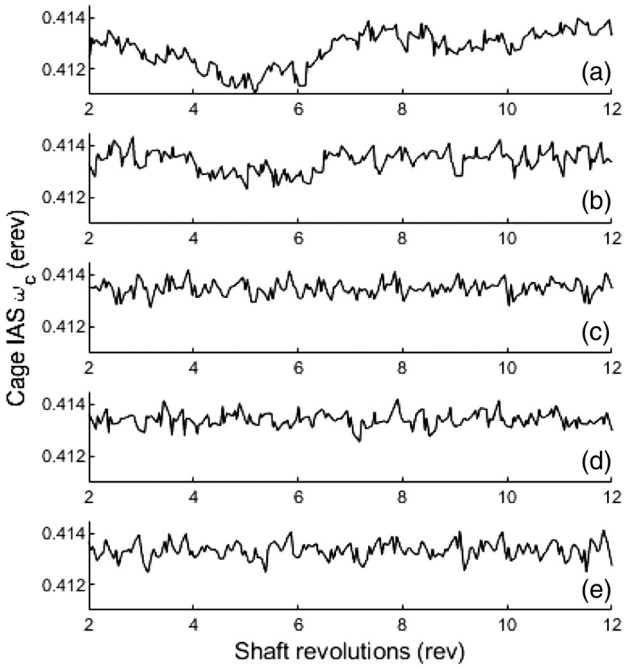

Fig. 7. Cage IAS signal for different shaft angular speeds. a) $\omega_s = 5$ Hz; b) $\omega_s = 10$ Hz; c) $\omega_s = 15$ Hz; d) $\omega_s = 20$ Hz; e) $\omega_s = 25$ Hz.

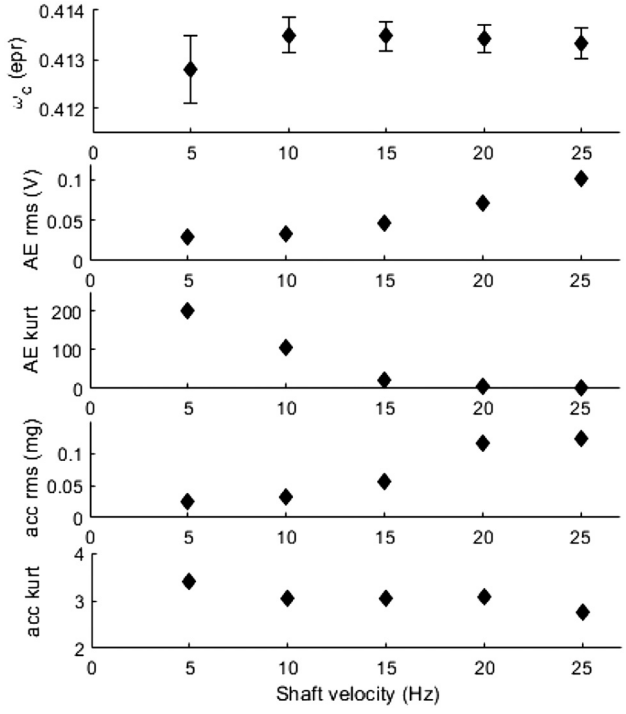

Fig. 8. Statistical features for test A. From top to bottom: ω_c (with error bands representing ±1 standard deviation), AE rms, AE kurtosis, acceleration rms, acceleration kurtosis.

for $\omega_s = 5\ Hz$ and $\omega_s = 25\ Hz$. The impulses are clearly seen for $\omega_s = 5\ Hz$, whereas for $\omega_s = 25\ Hz$ the signal has increased power but less impulsivity. Fig. 8 shows that the rms value of the AE and acceleration signals increases with

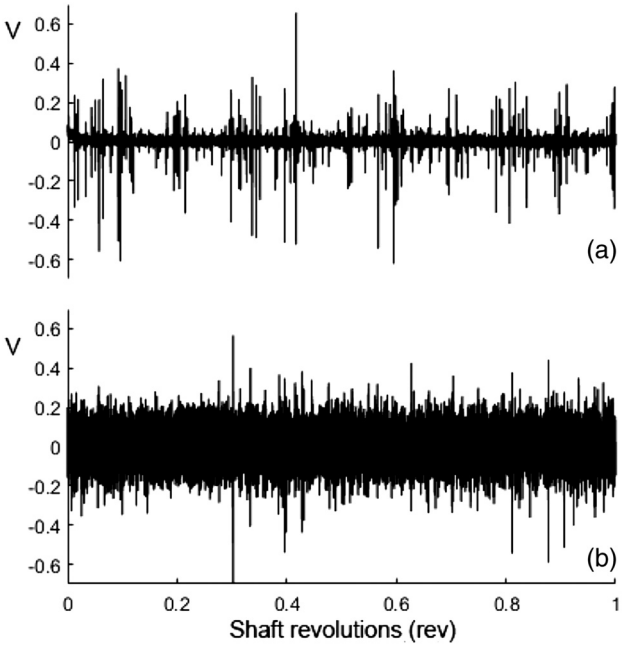

Fig. 9. AE signals. a) $\omega_s = 5$ Hz; b) $\omega_s = 25$ Hz.

the speed, indicating increased dissipated energy in the contacts. According to Cornel et al. [6], the AE amplitude increases with diminishing Λ and increases with increasing shaft speed, being the latter the dominant parameter. The same behavior is observed in the present test.

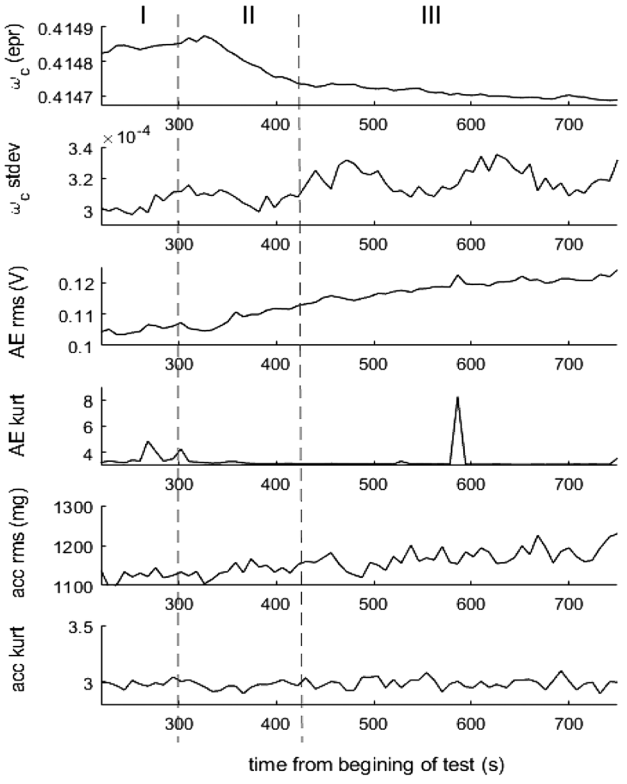

Fig. 10. Statistical features for test B. From top to bottom: ω_c mean value, ω_c standard deviation, AE rms, AE kurtosis, acceleration rms, acceleration kurtosis.

According to previous works [24], skidding is expected to become severe at high-speed and low-load conditions. Skidding should be detected as a variation of the cage IAS. This variation is not seen in Fig. 8, indicating that skidding does not occur under the tested conditions at $\omega s = 15$–25 Hz probably due to the relatively high load and medium speeds. Finally, the kurtosis of acceleration signal remains almost constant in all cases, probably due to the high-frequency characteristics of the impulses laying outside the measurement chain frequency band.

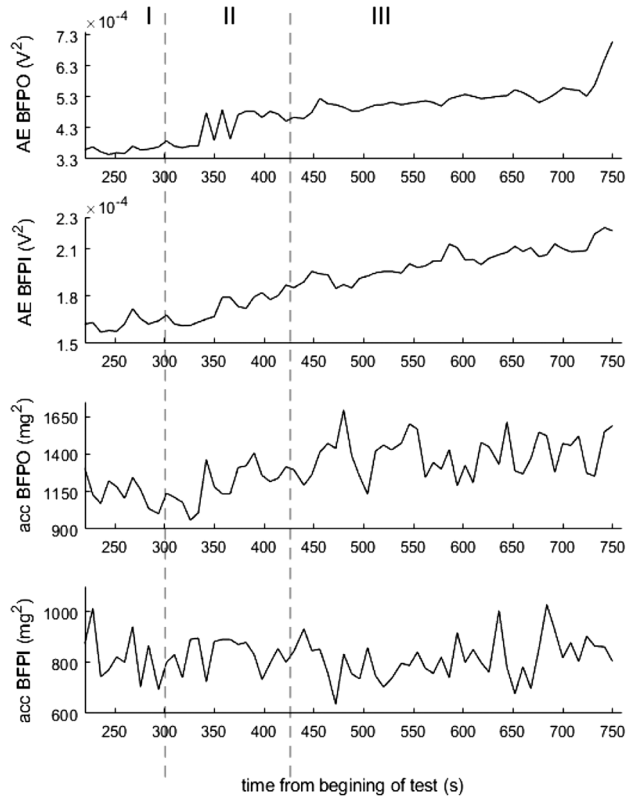

Fig. 11. Amplitudes for characteristic RB frequencies from the EES in test B. Top two: AE signal. Bottom two: accelerometer signal.

B. TEST B RESULTS: LUBRICANT DEPLETION

Figs. 10 and 11 present the evolution of the most relevant signal features computed for this test. The test started at time $t = 0$ s. The period $t = 0$–300 s was used for warm-up and baseline measurement. In $t = 300$ s, the orifice in the bearing housing was opened for the lubricant to exit. By $t = 420$ s, all the lubricant had been expelled. In Figs. 10 and 11, these time periods are noted as I, II, and III, respectively.

From $t = 200$ s up to the beginning of lubricant loss at $t = 300$ s, all features remain almost constant as expected. During the first 40 s of lubricant loss, all the parameters remain constant except for ω_c which increases slightly. This is probably due to a reduced drag force of the lubricant over the cage and rotating elements, while there is still enough lubricant in the contacting surfaces to maintain the same lubrication regime. For $t = 340$ s up to $t = 420$ s, we can see that ω_c continuously decreases and both the rms and the EES peaks clearly increase. This is consistent with a mixed lubrication regime where Λ is diminishing due to lubricant starvation. The traction forces increase leading to increased energy dissipation, thus decreasing the cage IAS and increasing the AE power. For time period III during which all the lubricant has been expelled, boundary lubrication is present at the contacting surfaces and ω_c continues to decrease but with a decreased slope. For the AE signal, both the rms and the EES peaks clearly increase, showing good correlation with the change in ω_c. Besides a high value at $t = 580$ s (probably an outlier), no change in the kurtosis is evidenced

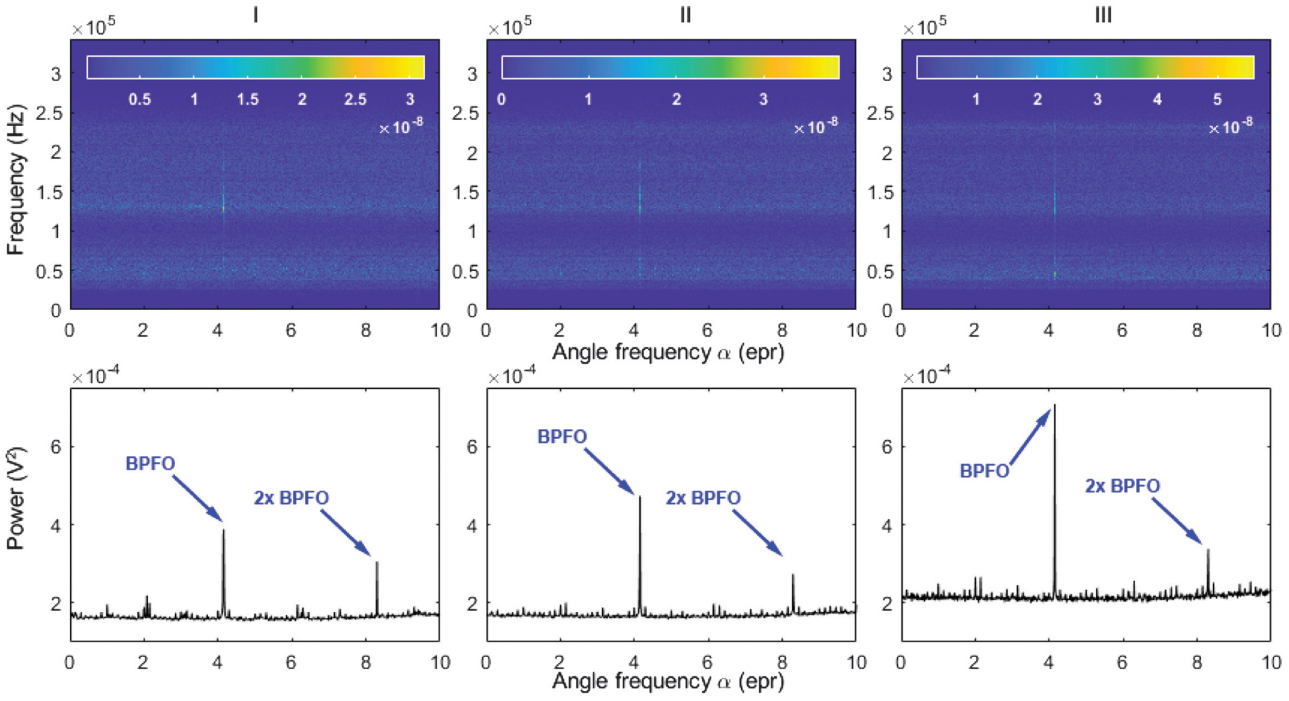

Fig. 12. SC (top) and EES (Bottom) for selected AE signals in the phases I, II, and III of test B.

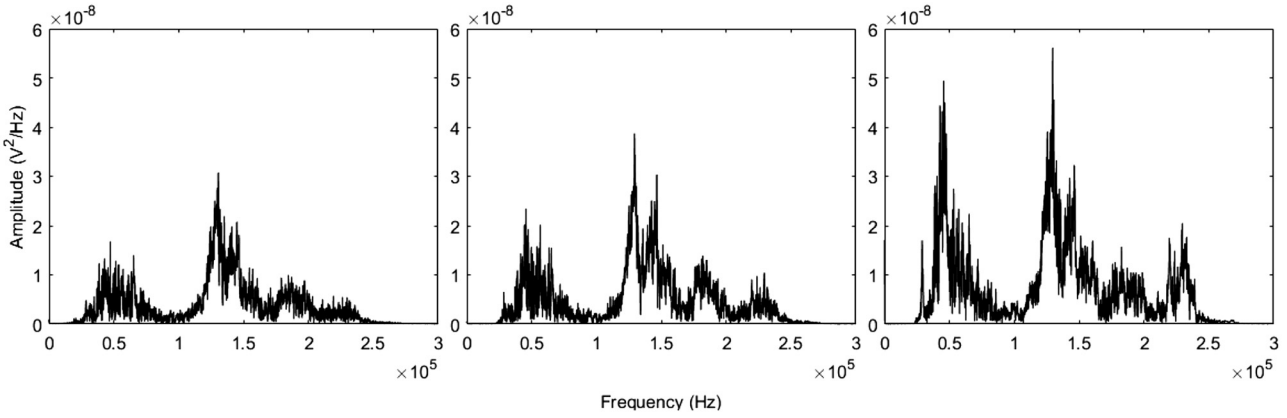

Fig. 13. Cyclic spectrum for α = BPFO. for selected AE signals in the phases I, II, and III of test B.

for $t > 300$ s. The signal from the accelerometer provides no signs of the change of lubrication regime. Neither the statistical parameters (rms, kurtosis) nor the EES peaks show any meaningful change. This indicates that the contacting surfaces of the REB emit mechanical energy at a higher frequency than that measured by the accelerometer.

Fig. 12 presents the SC and the EES for a selected signal of each time period. Fig. 13 shows the respective cyclic spectrum calculated for angle frequency $\alpha = BPFO$.

From Fig. 12, it is clear that measured AE energy is mainly modulated by the balls – outer race interaction (BPFO and harmonics). Also in this test, it was found that the modulated AE amplitude increases with diminishing Λ (i.e., lubricant starvation reduces the film thickness), in line with published results [6]. The AE cyclic spectrum at $\alpha = BPFO$ (Fig. 13) shows that the change in the energy associated with the ball-outer race interaction is mainly concentrated in the frequency bands 40–80, 120–150, and 220–240 kHz. Whether this is due to the AE generation itself or due to the transmission path could be a motive of further investigation.

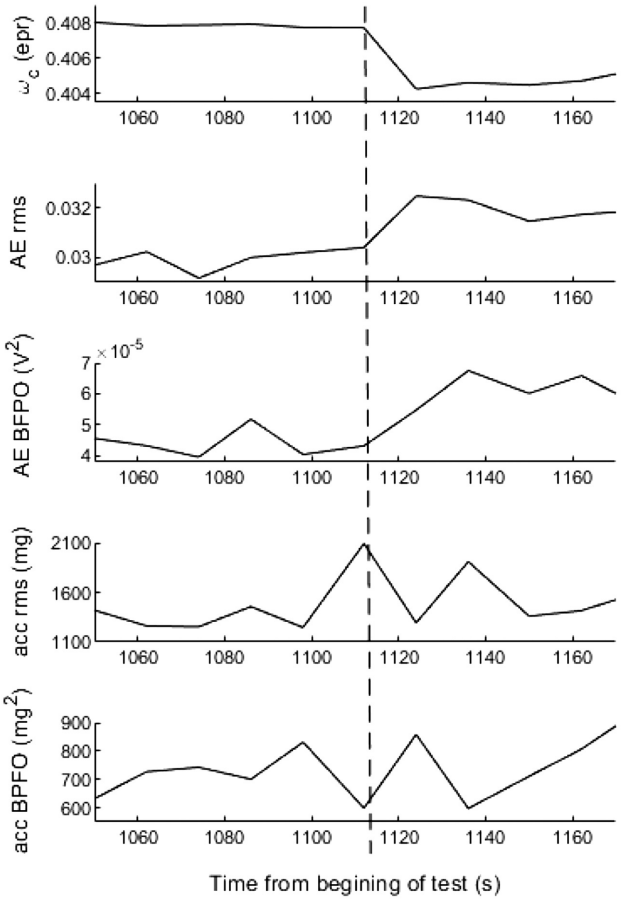

Fig. 14. Selected features for test C. The dotted line indicates the instant of misalignment.

C. TEST C RESULTS: MISALIGNMENT

Fig. 14 presents the evolution of the most relevant signal features computed for this test. After a warm-up, the misalignment is imposed at time $t = 1115$ s

It is seen that misalignment affects the cage IAS and AE features, but it is not detected by the accelerometer rms with the parameters shown. Fig. 15 presents the AE signal EES before and after misalignment, with BFPO power being the main difference. It is worth noting that in this test rig the

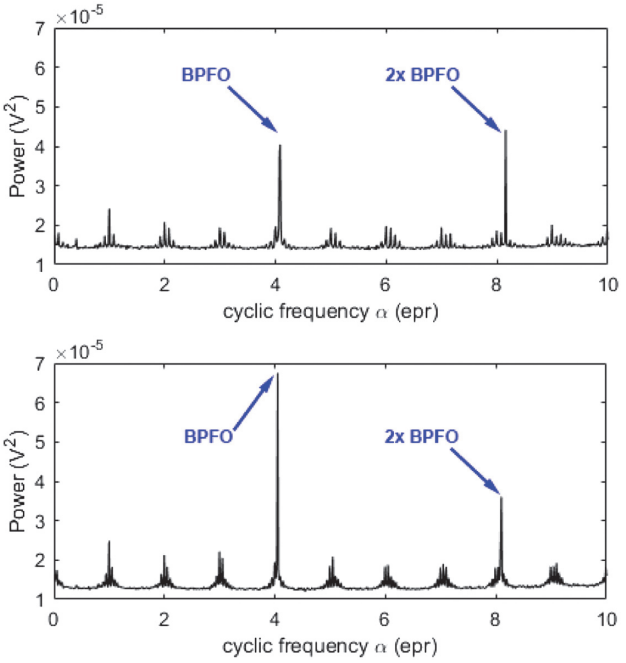

Fig. 15. EES before (top) and after (bottom) misalignment.

imposed misalignment can be detected by analyzing the low-frequency spectrum of the acceleration signal (1X/2X relation) because the applied torque modifies the rotor dynamic behavior. However, in a more complex mechanism, misalignment of the outer ring may not significantly affect the dynamics of the rotor, while still being detrimental to the bearing. The proposed method would cover this case.

V. CONCLUSIONS

The ω_c/ω_s ratio and the modulated AE energy serve as indicators of the lubrication regime. A simple instrumentation for online measurement of the cage IAS has been presented. This study shows, with a first experimental approach, that the cage IAS analysis in conjunction with AE analysis could be a suitable and powerful CM method for lubrication status and alignment condition of REBs. The method was capable of early and fast detection of misalignment and lubrication faults, whereas traditional broadband vibration analysis was unable to do so.

The presented IAS and AE measurement principles can be further developed for industrial applications. The presented IAS measurement and analysis method is simple and could be implemented in embedded systems for real-time monitoring, which makes it particularly interesting for integration in smart bearings and Industry 4.0 applications.

CONFLICT OF INTEREST STATEMENT

The authors declare no conflicts of interest.

REFERENCES

1. D. Dyer and R. M. Stewart, "Detection of rolling element bearing damage by statistical vibration analysis," *J Mech Des N Y*, vol. 100, no. 2, 229–235, 1978.
2. O. García Peyrano, V. Suedmacsen, W. Reimche, and D. Stegemann, "Non destructive control of ball and roller bearing damage using vibration analysis," *Practical review of industrial control*, vol. 26, no. 144, 26–30, 1987.
3. R. B. Randall and J. Antoni, "Rolling element bearing diagnostics—a tutorial," *Mech. Syst. Signal Process.*, vol. 25, no. 2, 485–520, 2011.
4. C. Malla and I. Panigrahi, "Review of condition monitoring of rolling element bearing using vibration analysis and other techniques," *J. Vib. Eng. Technol.*, vol. 7, no. 4, 407–414, 2019.
5. SKF Group, "Bearing damage and failure analysis," PUB BU/I3 14219/2 EN 2017. [Online]. Available: www.skf.com/binaries/pub12/Images/0901d1968064c148-Bearing-failures---14219_2-EN_tcm_12-297619.pdf
6. D. Cornel, F. Gutiérrez Guzmán, G. Jacobs, and S. Neumann, "Condition monitoring of roller bearings using acoustic emission," *Wind Energ. Sci.*, vol. 6, no. 2, 367–376, 2021.
7. P. Feng, P. Borghesani, W. A. Smith, R. B. Randall, and Z. Peng, "A review on the relationships between acoustic emission, friction and wear in mechanical systems," Appl. Mech. Rev., vol. 72, no. 2, 2019. doi: https://doi.org/10.1115/1.4044799.
8. P. Borghesani, W. A. Smith, X. Zhang, P. Feng, J. Antoni, and Z. Peng, "A new statistical model for acoustic emission signals generated from sliding contact in machine elements," *Tribol. Int.*, vol. 127, 412–419, 2018.
9. J. Antoni, "Cyclostationarity by examples," *Mech. Syst. Signal Process.*, vol. 23, no. 4, 987–1036, 2009.
10. J. Antoni, G. Xin, and N. Hamzaoui, "Fast computation of the spectral correlation," *Mech. Syst. Signal Process.*, vol. 92, 248–277, 2017.
11. M. Marticorena, R. Mayer, J. Vignolo, and O. García Peyrano, "Torsional vibration analysis applied for centrifugal pump condition monitoring," in Advances in Asset Management and Condition Monitoring, A. Ball, L. Gelman, and B. K. N. Rao, Eds. Switzerland: Smart Innovation, Systems and Technologies: Springer International Publishing, pp. 871–881, 2020. [Online]. Available: https://link.springer.com/book/10.1007/978-3-030-57745-2.
12. A. A. Gubran and J. K. Sinha, "Shaft instantaneous angular speed for blade vibration in rotating machine," *Mech. Syst. Signal Process.*, vol. 44, no. 1, 47–59, 2014.
13. J. Yang, L. Pu, Z. Wang, Y. Zhou, and X. Yan, "Fault detection in a diesel engine by analysing the instantaneous angular speed," *Mech. Syst. Signal Process.*, vol. 15, no. 3, 549–564, 2001.
14. A. Alwodai, F. Gu, and A. D. Ball, "A comparison of different techniques for induction motor rotor fault diagnosis," J. Phys.: Conf. Series, vol. 364, 2012. [Online]. Available: https://iopscience.iop.org/article/10.1088/1742-6596/364/1/012066.
15. L. Renaudin, F. Bonnardot, O. Musy, J. B. Doray, and D. Rémond, "Natural roller bearing fault detection by angular measurement of true instantaneous angular speed," *Mech. Syst. Signal Process.*, vol. 24, no. 7, 1998–2011, 2010.
16. Y. Wang, B. Tang, Y. Qin, and T. Huang, "Rolling bearing fault detection of civil aircraft engine based on adaptive estimation of instantaneous angular speed," *IEEE Trans. Ind. Inf.*, vol. 16, no. 7, 4938–4948, 2020.
17. Y. Li, F. Gu, G. Harris, A. Ball, N. Bennett, and K. Travis, "The measurement of instantaneous angular speed," *Mech. Syst. Signal Process.*, vol. 19, no. 4, 786–805, 2005.
18. H. André, F. Girardin, A. Bourdon, J. Antoni, and D. Rémond, "Precision of the IAS monitoring system based on the elapsed time method in the spectral domain," *Mech. Syst. Signal Process.*, vol. 44, no. 1, 14–30, 2014.
19. A. B. Jones, "A general theory for elastically constrained ball and radial roller bearings under arbitrary load and speed conditions," *J. Basic Eng.*, vol. 82, no. 2, 309–320, 1960.
20. T. A. Harris, "An analytical method to predict skidding in high speed roller bearings," *ASLE Trans.*, vol. 9, no. 3, 229–241, 1966.
21. W. Zhang, S. Deng, G. Chen, and Y. Cui, "Impact of lubricant traction coefficient on cage's dynamic characteristics in high-speed angular contact ball bearing," *Chin. J. Aeronaut.*, vol. 30, no. 2, 827–835, 2017.
22. S. Schwarz, H. Grillenberger, S. Tremmel, and S. Wartzack, "Investigations on the rolling bearing cage dynamics with regard to different operating conditions and cage properties," *IOP Conf. Series: Mater. Sci. Eng.*, vol. 1097, no. 1, 2021. [Online]. Available: https://iopscience.iop.org/article/10.1088/1757-899X/1097/1/012009.
23. T. Nogi, K. Maniwa, and N. Matsuoka, "A dynamic analysis of cage instability in ball bearings," *J Tribol*, vol. 140, no. 1, 2017. doi: https://doi.org/10.1115/1.4036451.
24. S. Gao, S. Chatterton, P. Pennacchi, Q. Han, and F. Chu, "Skidding and cage whirling of angular contact ball bearings: Kinematic-Hertzian contact-thermal-elasto-hydrodynamic model with thermal expansion and experimental validation," *Mech. Syst. Signal Process.*, vol. 166, 2022. doi: https://doi.org/10.1016/j.ymssp.2021.108427.

25. J. Takabi and M. M. Khonsari, "On the influence of traction coefficient on the cage angular velocity in roller bearings," *Tribol. Trans.*, vol. 57, no. 5, 793–805, 2014.
26. S. Chen, X. Chen, Q. Li, and J. Gu, "Experimental study on cage dynamic characteristics of angular contact ball bearing in acceleration and deceleration process," *Tribol. Trans.*, vol. 64, no. 1, 42–52, 2021.
27. D. Rémond, J. Antoni, and R. B. Randall, "Editorial for the special issue on instantaneous angular speed (ias) processing and angular applications," *Mech. Syst. Signal Process.*, vol. 44, no. 1, 1–4, 2014.
28. B. J. Hamrock and D. Dowson, "Isothermal elastohydrodynamic lubrication of point contacts: Part iii—fully flooded results," *J. Lubr. Technol.*, vol. 99, no. 2, 264–275, 1977.
29. M. Masjedi and M. M. Khonsari, "On the effect of surface roughness in point-contact EHL: Formulas for film thickness and asperity load," *Tribol. Int.*, vol. 82, 228–244, 2015.
30. J. A. Greenwood, "Elastohydrodynamic lubrication," *Lubricants*, vol. 8, no. 5, 2020. [Online]. Available: https://www.mdpi.com/2075-4442/8/5/51.